Received: 6 July 2020 | Revised: 14 January 2021 | Accepted: 28 February 2021

DOI: 10.1111/ejn.15189

RESEARCH REPORT

EJN European Journal of Neuroscience FENS WILEY

Impaired posterior cingulate cortex–parahippocampus connectivity is associated with episodic memory retrieval problems in amnestic mild cognitive impairment

Sven Vanneste[1,2,3] | **Alison Luckey**[2,3] | **S. Lauren McLeod**[1] | **Ian H. Robertson**[2,3] | **Wing Ting To**[4]

[1]Lab for Clinical & Integrative Neuroscience, School of Behavioral and Brain Sciences, The University of Texas at Dallas, Richardson, TX, USA

[2]School of Psychology, Trinity College Dublin, Dublin, Ireland

[3]Global Brain Health Institute & Institute of Neuroscience, Trinity College Dublin, Dublin, Ireland

[4]School of Nursing, Trinity College Dublin, Dublin, Ireland

Correspondence
Sven Vanneste, Lab for Clinical & Integrative Neuroscience, School of Psychology, Global Brain Health Institute, Institute of Neuroscience, Trinity College Dublin, College Green 2, Dublin, Ireland.
Email: sven.vanneste@tcd.ie

Abstract

Episodic memory retention and retrieval decline are the most common impairments observed in amnestic mild cognitive impairment (aMCI) patients who progress to Alzheimer's disease (AD). Clinical electroencephalography research shows that patients with dementia due to AD exhibit a slowing of neural electrical activity in the parietal cortex. Memory research has further suggested that successful memory performance is associated with changes in a posterior cingulate–parahippocampal cortical network together with increased θ–γ oscillatory coupling, where θ oscillations act as carrier waves for γ oscillations, which contain the actual information. However, the neurophysiological link between the memory research and clinical studies investigating aMCI and AD is lacking. In this study, we look at brain activity in aMCI and how it relates to memory performance. We demonstrate decreased γ power in the posterior cingulate cortex and the left and right parahippocampus in aMCI patients in comparison to control participants. This goes together with reduced θ coherence between the posterior cingulate cortex and parahippocampus associated with altered memory performance aMCI patients in comparison to control participants. In addition, comparing patients with aMCI to control participants reveals an effect for θ–γ coupling for the posterior cingulate cortex, and the left and right parahippocampus. Taken together, our results show that parahippocampus and posterior cingulate cortex interact via θ–γ coupling, which is associated with memory recollection and is altered in aMCI patients, offering a potential candidate mechanism for memory decline in aMCI.

KEYWORDS

amnestic mild cognitive impairment, gamma, memory, posterior cingulate cortex, theta

Abbreviations: AD, Alzheimer's disease; aMCI, amnestic mild cognitive impairment; BAI, Beck Anxiety Inventory; BDI, Beck Depression Inventory; CVLT, California Verbal Learning Test II; D-KEFS, Delis–Kaplan Color Word Interference Test; EEG, Electroencephalography; eLORETA, Exact low-resolution brain electromagnetic tomography; MMSE, Mini Mental state Examination; PCC, posterior cingulate cortex.

Edited by: John Foxe

1 | INTRODUCTION

Amnestic mild cognitive impairment (aMCI) is a prodromal stage of Alzheimer's disease (AD) (Petersen & Negash, 2008), part of a continuum comprised of a lengthy preclinical stage, a middle stage of aMCI, and a final stage of dementia (Sperling et al., 2011). The prevalence of MCI is 10%–20% in adults aged 65 years or older and more than 50% of MCI patients progress to dementia within 5 years (Langa & Levine, 2014). Episodic memory retention and retrieval decline are the most common impairments in the MCI patients who progress to AD (Summers & Saunders, 2012). Even mild deficits of this sort cause great distress to affected patients, who feel that their autonomy, independence, and ability to lead high-quality lives are negatively affected (Voytek & Gazzaley, 2013). Such impairments are often considered the most debilitating aspect of aging and have drawn great attention from clinicians and society at large.

The pathophysiology of AD has been associated with dysfunction resulting from synaptic toxicity of amyloid β, supposedly occurring early in the cascade of events that eventually leads to the progressive dysfunction of neural networks controlling memory processes (Sperling et al., 2013). Functional MRI studies have correlated increased amyloid-β burden in clinically normal adults both with reduced resting-state functional connectivity (Drzezga et al., 2011; Elman et al., 2016; Hedden et al., 2009) and neural activation in the brain regions underpinning memory, including the (para)hippocampus and posterior cingulate cortex (PCC) (Kennedy et al., 2012; Mormino et al., 2012; Oh & Jagust, 2013). Electroencephalography (EEG), a more clinically robust method to capture in vivo synaptic functioning, has further shown a slowing of brain electrical activity reflected in an increased proportion of relatively slow-wave resting oscillations, including the theta range (4–8 Hz; θ power) (Cohen, 2017; van Straaten et al., 2014). This is followed in later stages by a decrease in the proportion of resting oscillations in the alpha range (8–13 Hz; α power) in patients with dementia due to AD (van Straaten et al., 2014). At the aMCI stage, EEG abnormalities are expected to be in an intermediate state between healthy controls and dementia patients (Gouw et al., 2017; van der Hiele et al., 2007).

Memory research has suggested that successful episodic memory retrieval is associated with enhanced fMRI signal in neocortical areas including the PCC and (para)hippocampus/medial temporal lobe (Spaniol et al., 2009). Research using stereo-EEG further reported an increase in power in the gamma range of the EEG spectrum (30–70 Hz; γ power) during correct item retrieval in the PCC (Lega et al., 2017). These γ oscillations have been suggested to cause the (para) hippocampal reinstatement of memory representations in the PCC (Mormann et al., 2005; Nyhus & Curran, 2010). In humans, there is greater θ and γ power in the parahippocampus and posterior cortical regions for correctly remembered items (Addante et al., 2011; Nyhus & Curran, 2010). Additionally, the same two areas have been found to synchronize at θ frequencies during memory retrieval (Lega et al., 2017). Findings from event-related EEG studies provide evidence that θ–γ coupling goes together with successful memory retrieval, which is consistent with previous research suggesting that θ–γ coupling facilitates transfer of information throughout the entorhinal–hippocampal network (Colgin, 2015).

From a clinical point of view, episodic memory impairment is particularly relevant because it constitutes one of the hallmarks of AD. However, research has yet to establish a neurophysiological link between memory studies and clinical studies looking into aMCI and AD. The objective of this study is to investigate the effects of aMCI oscillatory activity using resting-state EEG. Resting-state measurements are a promising neuromarker for characterizing cognitive decline due to its capability of revealing features of intrinsic functional brain organization relevant to cognitive abilities and disease status (Gabrieli et al., 2015; Woo et al., 2017). Compared to traditional diagnostic tools such as, neuropsychological tests, resting state may be less demanding on the participant. In addition, resting state does not involve the presentation of stimuli and thus is easier to standardize and share across different study sites. Recent advancements demonstrate the exciting possibility of predicting an individual's cognitive abilities (e.g., sustained attention and fluid intelligence) from using resting state (Finn et al., 2015; Rosenberg et al., 2016; Shen et al., 2017). Furthermore, a recent study provides promising evidence that functional connectivity from a resting-state scan can reveal AD-related cognitive impairment in an aging population with health, MCI, and AD participants, which is potentially advantageous over administering standardized cognitive battery tests that can be challenging and time consuming (Lin et al., 2018). We hypothesize: (a) reduced γ power in aMCI patients compared to age- and gender-matched healthy participants; (b) reduced θ coherence between the PCC and parahippocampus in aMCI patients; (c) altered cross-frequency coupling between θ and γ in the PCC and parahippocampus in aMCI patients; and (d) altered episodic memory as measured with the California Verbal Learning Test (CVLT) – delayed recall that correlates with activity and functional connectivity in aMCI patients as well as for θ–γ coupling. This study can provide a neural mechanistic account of memory performance. Such knowledge will provide novel insights toward developing a biomarker.

2 | MATERIALS AND METHODS

Twenty aMCI patients and 20 healthy control participants matched for age and gender were enrolled. Participants were

recruited and screened, prior to inclusion in the study. Non-English speakers were excluded because not all the screening forms, questionnaires, and tests are available or validated in any language except for English. Patient participants enrolled in this study needed to be able to provide informed consent to participate in the study, have a confirmed aMCI diagnosis by a behavioral neurologist, and have their medication stable for at least 3 months prior to data collection. Exclusion criteria included: evidence of any psychiatric disorder, currently participating in another clinical study, medication contra-indications or contra-indications for EEG, past or current alcohol and/or drug abuse, severe uncontrolled organic disease, use of pacemaker, history of seizures, history of major head trauma, history of neurosurgery, and cerebral metallic artifacts. The aMCI patients who were referred to the study were screened for clinical secondary causes of dementia or cognitive deficits, such as diabetes, hypothyroidism, SIDA, vitamin B12 and folate deficiency, excessive alcohol consumption, syphilis, and risk factors for cardiovascular disease, such as atherosclerosis and diabetes, focal or lacunar ischemia, expansive brain tumors, depression, and hydrocephalus. The study was conducted as approved by the Institutional Review Board of the University of Texas at Dallas and all participants signed an informed consent. Data are available upon request.

2.1 | aMCI Group

Twenty participants, ages 55–70 years, with education level ≥4 years, meeting clinical/neuropsychological criteria for aMCI for at least 1 year, and with a Mini Mental state Examination (MMSE) score of less than 25.

2.2 | Healthy Control Group

Twenty participants, ages 55–70 years, education level ≥4 years, otherwise conforming to inclusion criteria for study and with a MMSE score of more than 27.

All participants were administered the Beck Depression Inventory (BDI) and Beck Anxiety Inventory (BIA) scales which, although not a diagnostic instrument, allows comparison of the two groups on mood as well as on other measures. See Figure 1 for demographic overview.

2.3 | Assessments

2.3.1 | California Verbal Learning Test II (CVLT-II)

A measure of episodic verbal learning and memory that demonstrates sensitivity to a range of clinical conditions. The test attempts to link memory deficits with impaired performance on specific tasks. It assesses encoding, recall, and recognition in a single modality of item presentation. The CVLT is a more sensitive measure of episodic memory than other verbal learning tests. The CVLT-II quantifies recall and recognition of two-word lists over several immediate and delayed memory trials. The participant is asked to recall words from List A immediately after each presentation of the list in the first five learning trials. List A consists of 16 words, with four words from each of the four semantic categories. A 16-word interference list (List B) is then presented for one trial, and followed by the short-delay free-recall and short-delay cued-recall trials of List A. After a 20-min delay, the long-delay free recall, long-delay cued recall, and yes/no recognition trials of List A are administered. The CVLT-II also includes an optional forced-choice recognition trail, which may be administered after another 10-min delay.

2.3.2 | Delis Kaplan Color Word Interference Test (D-KEFS)

A battery of neuropsychological tests designed to measure executive functions. D-KEFS exists out of different subscales: involves a series of four conditions: color naming, word reading, inhibition, and inhibition switching (Delis et al., 2001).

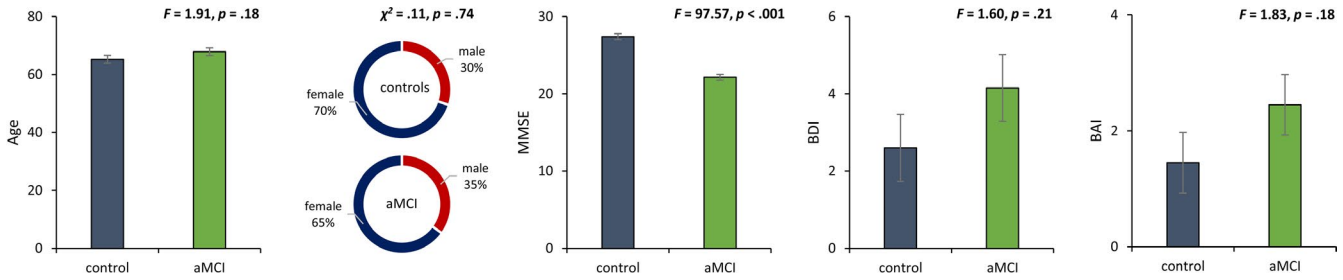

FIGURE 1 No difference between aMCI patients and control participants for age, gender, BDI, and BAI, while a significant reduced score was demonstrated for aMCI patients in comparison to control participants on the MMSE

2.4 | EEG collection and processing

2.4.1 | Data collection

Electroencephalography data (Neuroscan, http://compumedicsneuroscan.com/) were obtained in a quiet room while each participant was sitting upright in a comfortable chair. The scalp was cleaned with alcohol wipes before the baseline EEG recording. The EEG was sampled with 64 electrodes in the standard 10–20 International placement and impedances were checked to remain below 5 kΩ. Eyes-closed resting-state EEG was collected (sampling rate = 1 kHz, band passed DC–200 Hz) over the duration of approximately 5 min. The midline reference was located at the vertex and the ground electrode was located at AFZ. Participants were instructed not to drink alcohol 24 hr prior to EEG recording or caffeinated beverages 1 hr before recording to avoid alcohol- or caffeine-induced changes in the EEG stream (Logan et al., 2002; Siepmann & Kirch, 2002; Volkow et al., 2000). Participant alertness was checked by monitoring both slowing of the α rhythm and appearance of spindles in the EEG stream to prevent possible enhancement of the θ power due to drowsiness during recording (Moazami-Goudarzi et al., 2010). No recordings needed to be stopped because drowsiness and no participants needed to be excluded.

Off-line data were resampled to 128 Hz, band-pass filtered in the range 2–44 Hz, and subsequently transposed into Eureka! software (Congedo, 2002), and plotted and carefully inspected for manual artifact-rejection. All episodic artifacts or ECG artifact were removed from the stream of the EEG. An artifact was defined as an EEG characteristic that differs from signals generated by activity in the brain. (1) Some artifacts are known to be in a limited frequency range, e.g., above some frequency. These were removed by frequency filtering. (2) Some artifacts consisted of discrete frequencies such as 50 Hz (or 60 Hz for USA) or its harmonics. These were removed by notch filtering. (3) Some artifacts are limited to a certain time range, e.g., in the case of eye blinks. These artifacts were recognized by visual inspection and these time intervals were discarded. (4) Some artifacts originated from one or a few distinct sources or a limited volume of space so that the artifact topography is a superposition of characteristic topographies (equivalently, the artifact is limited to a subspace of the signal space). We removed these artifacts by determining the characteristic topographies (equivalently, the artifact subspace), so that the remaining signals do not contain anything from the artifact subspace. (5) Artifacts that are independent from true brain signals based on independent component analysis were removed. (6) Some artifacts are characterized by a particular temporal pattern such as exponential decay. We removed these artifacts by modeling the artifact and fitting its parameters to the data and then removing the artifact. Average Fourier cross-spectral matrices were computed for frequency bands δ (2–3.5 Hz), θ (4–7.5 Hz), α (8–12 Hz), β (13–30 Hz), and γ (30.5–44 Hz).

2.4.2 | Source localization

Exact low-resolution brain electromagnetic tomography (eLORETA) (Jatoi et al., 2014; Pascual-Marqui, 2002; Pascual-Marqui et al., 2011) was used to estimate the intracerebral electrical sources. As a standard procedure, a common average reference transformation (Pascual-Marqui, 2002) is performed before applying the eLORETA algorithm. eLORETA computes neuronal electrical activity as current density (A/m^2) without assuming a predefined number of active sources. The solution space used in this study and associated lead-field matrix are those implemented in the LORETA-Key software (freely available at http://www.uzh.ch/keyinst/loreta.htm). This software implements revisited realistic electrode coordinates (Jurcak et al., 2007) and the lead field produced applying the boundary element method on the MNI-152 (Montreal Neurological Institute, Canada) template (Fuchs et al., 2002). The eLORETA-key anatomical template divides and labels the neocortical (including parahippocampus and anterior cingulate cortex) MNI-152 space in 6,239 voxels of dimension 5 mm^3, based on probabilities returned by the Demon Atlas (Lancaster et al., 2000). The co-registration makes use of the correct translation from the MNI-152 space into the Talairach and Tournoux space.

2.4.3 | Region of interest

The log-transformed electric current density was calculated for the regions of interest (ROIs) for the different frequency bands: θ (4–7.5 Hz) and γ (30.5–44 Hz). The ROIs in the present study are PCC, left parahippocampus, and right parahippocampus. For the PCC, we do not differentiate between left and right due to their proximity to the midline. Due to volume conduction, laterality is harder to differentiate for areas close to the midline. The selection of these regions of interest was based on our a priori hypothesis that they would be affected in aMCI relative to healthy controls.

2.4.4 | Lagged phase coherence

Coherence and phase synchronization between time series corresponding to different spatial locations are usually interpreted as indicators of connectivity. However, any measure of dependence is highly contaminated with an instantaneous,

non-physiological contribution due to volume conduction (Pascual-Marqui, 2007). However, Pascual-Marqui (Pascual-Marqui, 2007) introduced new measures of coherence and phase synchronization taking into account only non-instantaneous (lagged) connectivity, effectively removing the confounding factor of volume conduction. Such lagged phase coherence between two sources can be interpreted as the amount of crosstalk between the regions contributing to the source activity (Congedo et al., 2010). As the two components oscillate coherently with a phase lag, the crosstalk can be interpreted as information sharing by axonal transmission. More precisely, the discrete Fourier transform decomposes the signal in a finite series of cosine and sine waves at the Fourier frequencies (Bloomfield, 2013). The lag of the cosine waves with respect to their sine counterparts is inversely proportional to their frequency and amounts to a quarter of the period; for example, the period of a sinusoidal wave at 10 Hz is 100 ms. The sine is shifted a quarter of a cycle (25 ms) with the respect to the cosine. Then, the lagged phase coherence at 10 Hz indicates coherent oscillations with a 25 ms delay, while at 20 Hz the delay is 12.5 ms, etc. The threshold of significance for a given lagged phase coherence value according to asymptotic results can be found as described by Pascual-Marqui (2007), where the definition of lagged phase coherence can be found as well. As such, this measure of dependence can be applied to any number of brain areas jointly, i.e., distributed cortical networks, whose activity can be estimated with sLORETA. Measures of linear dependence (coherence) between the multivariate time series are defined. The measures are non-negative and take the value zero only when there is independence and are defined in the frequency domain: δ (2–3.5 Hz), θ (4–7.5 Hz), α (8–12 Hz), β (13–30 Hz), and γ (30.5–44 Hz).

Based on this principle, lagged linear connectivity was calculated. Time series of current density were extracted for different region of interests using eLORETA. Power in all 6,239 voxels was normalized to a power of 1 and log transformed at each time point. Region-of-interest values thus reflect the log-transformed fraction of total power across all voxels, separately for specific frequencies. Regions of interest selected were the PCC, left parahippocampus, and right parahippocampus.

2.4.5 | Cross-frequency coupling and long-range phase–amplitude coupling

Θ–γ coupling is proposed to be an effective manner of communication between cortically distant areas (Canolty et al., 2006). To verify whether this coupling is present, it was calculated for the PCC, the left parahippocampus, and the right parahippocampus using phase–amplitude cross-frequency coupling. Phase–amplitude was chosen over power–power cross-frequency coupling as the former has been shown to reflect a physiological mechanism for effective communication in the human brain (Canolty et al., 2006). Coupling was computed by first obtaining the time series for the x, y, and z components of the eLORETA current for the voxel of each ROI. These are the time series of the electrical current in the three orthogonal directions in space. Next, these were filtered in the θ (4–7.5 Hz) and γ (30.5–44 Hz) frequency band-pass regions. In each frequency band and for each ROI, a principal component analysis for the overall x, y, z component was computed, and the first component was retained for the θ and γ bands. The Hilbert transform was then computed on the γ component and the signal envelope retained. Finally, the Pearson correlation was computed for each individual between the θ component and the envelope of the γ component for each region of interest.

In addition, we also calculated long-range phase–amplitude coupling between the PCC and the left parahippocampus, and between the PCC and the right parahippocampus. Similarly, as for cross-frequency coupling, the time series for the x, y, and z components of the eLORETA current for the voxel of each ROI were calculated. The signal was then filtered in the θ (4–7.5 Hz) and γ (30.5–44 Hz) frequency band-pass regions. The principal component analysis for the overall x, y, and z component was computed for each region, and the first component was retained for the θ and γ bands. The Hilbert transform was then computed on the γ component and the signal envelope retained. Finally, the Pearson correlation was computed for each individual between the θ component of the left and right parahippocampus and the envelope of the γ component for the PCC.

2.5 | Statistical analyses

2.5.1 | Whole-brain analysis

The methodology used is a non-parametric permutation test. It is based on estimating, via randomization, the empirical probability distribution for the max-statistic under the null hypothesis comparisons (Nichols & Holmes, 2002). This methodology corrects for multiple testing (i.e., for the collection of tests performed for all voxels, and for all frequency bands). Due to the non-parametric nature of this method, its validity does not rely on any assumption of Gaussianity (Nichols & Holmes, 2002). The non-parametric approach has the advantage of being distribution independent as well as insensitive to extreme values over 6,239 voxels. Due to this approach, smoothness or removal of extreme values is not required. These whole-brain comparisons were performed by eLORETA through multiple voxel-by-voxel comparisons using a logarithm of F-ratio. The significance threshold for all tests was based on a permutation test with 5,000 permutations. Comparisons were made between the controls versus aMCI participants.

2.5.2 | Region-of-interest analysis

As we only look at a limited number of voxels, we performed a parametric test and test for normality. We applied MANOVA including the current density for the PCC, left parahippocampus, and right parahippocampus as dependent variables and group (control versus aMCI) as independent variables for the θ and γ frequency bands. If the outcome of the MANOVA was significant, a univariate ANOVA was conducted for the different regions separately. A correction for multiple correction using the Bonferroni method was applied to correct for the different univariate ANOVAs (Holm, 1979). In addition, we included a linear discriminant analysis (McLachlan, 2004), a method used in statistics and other fields, to find a linear combination of features that characterizes or separates two or more classes of objects or events – for γ frequency band including the current density for the PCC, the left and right parahippocampus to verify if these ROI can make differentiation between the aMCI and control participants.

If the θ or γ frequency band shows a significant finding, Pearson correlations were calculated between the region of interest (PCC, left parahippocampus, and right parahippocampus) and the CVLT-II overall score as well as the subscales *Free recall (list A)*, *Free recall (list B)*, *Short Recall (free recall)*, *Short Recall (cued recall)*, *Long-delay (free recall)*, *Long-delay (cued recall)*, and *Long-delay (recognition)* for the γ frequency band. For the D-KEFS, as well as the subscales *Color naming*, *Word reading*, *Inhibition,* and *Inhibition switching,* Pearson correlations were calculated with the regions of interest (PCC, left parahippocampus, and right parahippocampus) for the γ frequency band.

2.5.3 | Lagged phase coherence analysis

Lagged phase coherence or functional connectivity contrast was calculated for all frequency bands. The significance threshold was based on a permutation test with 5,000 permutations. This methodology corrects for multiple testing (i.e., for the collection of tests performed for all voxels, and for theta bands). Comparisons were made between the controls versus aMCI patients.

Only for the frequency band that was significant, correlations were calculated between the lagged phase coherence and CVLT-II overall score as well as the subscales *Free recall (list A)*, *Free recall (list B)*, *Short Recall (free recall)*, *Short Recall (cued recall)*, *Long-delay (free recall)*, *Long-delay (cued recall)*, and *Long-delay (recognition)* for the θ–γ coupling. In addition, correlation was calculated between the lagged phase coherence and for the D-KEFS, as well as the subscales *Color naming*, *Word reading*, *Inhibition*, and *Inhibition switching*.

2.5.4 | Phase-amplitude coupling and Long-Range Phase-amplitude coupling analysis

We performed a MANOVA including the θ–γ phase-amplitude coupling in the PCC, the left parahippocampus, and the right parahippocampus as dependent variables and group (control versus aMCI) as the independent variable. If the outcome of the MANOVA was significant, a univariate ANOVA was conducted for the different cross-frequency coupling separately, including the Bonferroni correction for multiple comparisons (Holm, 1979). A similar analysis will be applied for long-range phase-amplitude coupling, including the amplitude of the γ band of the PCC, and the θ phase of left and right parahippocampus as dependent variables and group (control versus aMCI) as the independent variable.

Pearson correlations were calculated between the region of interest (PCC, left parahippocampus, and right parahippocampus) and the CVLT-II overall score as well as the subscales *Free recall (list A)*, *Free recall (list B)*, *Short Recall (free recall)*, *Short Recall (cued recall)*, *Long-delay (free recall)*, *Long-delay (cued recall)*, and *Long-delay (recognition)* for the θ–γ coupling. For the D-KEFS, as well as the subscales *Color naming*, *Word reading*, *Inhibition*, and *Inhibition switching*, Pearson correlations were calculated with the region-of-interest PCC, left parahippocampus, and right parahippocampus for the θ–γ coupling. A similar analysis was applied for long-range phase–amplitude coupling.

3 | RESULTS

3.1 | Behavioral assessments

Overall, a significant difference was obtained for the CVLT-II ($F(1, 38) = 4.35$, $p = 0.044$, $\eta^2 = 0.10$) and the D-KEFS ($F(1, 38) = 8.65$, $p = 0.006$, $\eta^2 = 0.19$) between control participants (CVLT: 18.51 ± 3.22; D-KEFS: 44.18 ± 7.14) and patients with aMCI (CVLT: 16.02 ± 4.26; D-KEFS: 61.60 ± 25.51) (see Figure 2). Although the effect for the D-KEFS seems to be stronger than the CVLT-II, it is important to keep in mind that the CVLT-II has more subscales, which drive the effect.

For the CVLT-II, the effect was mainly driven by the *Free recall (list B)* ($F(1, 38) = 13.80$, $p = 0.001$, $\eta^2 = 0.27$), *Short Recall (free recall)* ($F(1, 38) = 9.00$, $p = 0.005$, $\eta^2 = 0.19$), *Long-delay (free recall)* ($F(1, 38) = 4.84$, $p = 0.034$, $\eta^2 = 0.11$), and *Long-delay (cued recall)* ($F(1, 38) = 4.96$, $p = 0.032$, $\eta^2 = 0.12$). For these subscales, we see a higher score for control participants in comparison to patients with aMCI. No significant difference was obtained between controls participants and patients with aMCI for *Free recall (list A)* ($F(1, 38) = 0.31$, $p = 0.58$, $\eta^2 = 0.008$), *Short Recall (cued recall)* ($F(1, 38) = 0.93$, $p = 0.34$, $\eta^2 = 0.02$), and *Long-delay*

(recognition) ($F(1, 38) = 4.04$, $p = 0.052$, $\eta^2 = 0.10$). See Figure 2 for an overview.

For the D-KEFS, an effect was obtained due to all subscales, showing a significant difference between controls participants and patients with aMCI for *Color naming* ($F(1, 38) = 5.41$, $p = 0.025$, $\eta^2 = 0.13$), *Word reading* ($F(1, 38) = 5.72$, $p = 0.022$, $\eta^2 = 0.13$), *Inhibition* ($F(1, 38) = 8.89$, $p = 0.005$, $\eta^2 = 0.19$), and *Inhibition switching* ($F(1, 38) = 6.20$, $p = 0.017$, $\eta^2 = 0.14$). For all these subscales, we see that aMCI participants take longer to complete the task in comparison to control participants. See Figure 2 for an overview.

3.2 | Neurophysiology

3.2.1 | Whole-brain analysis

A whole-brain analysis showed a significant decrease in γ power for patients with aMCI in comparison to control participants ($F = 1.91$, $p = 0.045$) in the PCC extending into the retrosplenial cortex and the parahippocampus (see Figure 3a). No significant effect was obtained when comparing patients with aMCI and control participants for the δ, θ, α, or β frequency bands.

3.2.2 | Region-of-interest analysis

A comparison including the PCC, the left and right parahippocampus between patients with aMCI in comparison to control participants revealed no significant effect for the θ frequency band ($F(3,36) = 2.13$, $p = 0.11$, $\eta^2 = 0.15$). Yet, a comparison between patients with aMCI and the control participants revealed a significant difference in current density for the γ frequency band ($F(3,36) = 4.87$, $p = 0.006$, $\eta^2 = 0.29$). For the PCC ($F(1,38) = 9.30$, $p = 0.004$, $\eta^2 = 0.20$), as well for the left parahippocampus ($F(1,38) = 8.24$, $p = 0.007$, $\eta^2 = 0.18$) and right parahippocampus ($F(1,38) = 13.34$, $p = 0.001$, $\eta^2 = 0.26$), a significant decrease in γ power was revealed for the patients with aMCI (PCC: 1.44 ± 1.10; left HIP: 1.69 ± 1.04; right HIP: 1.58 ± 0.98) in comparison to control participants (PCC: 2.32 ± 0.66; left HIP: 2.46 ± 0.59; right HIP: 2.51 ± 0.58). See Figure 3b for overview.

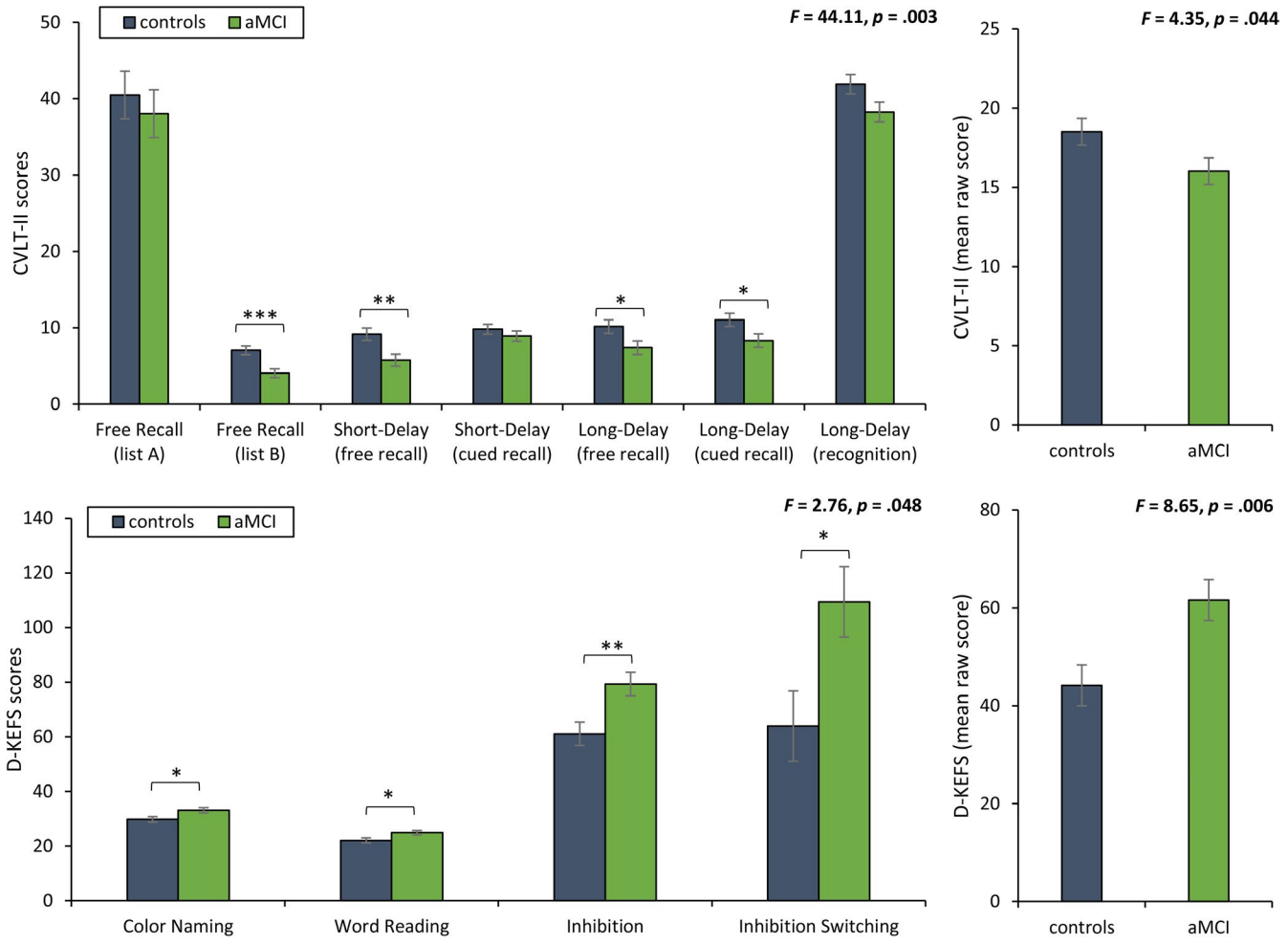

FIGURE 2 Behavioral assessments for the CVLT-II and D-KEFS subscale and mean total score. *$p < 0.05$; **$p < 0.01$; ***$p < 0.001$

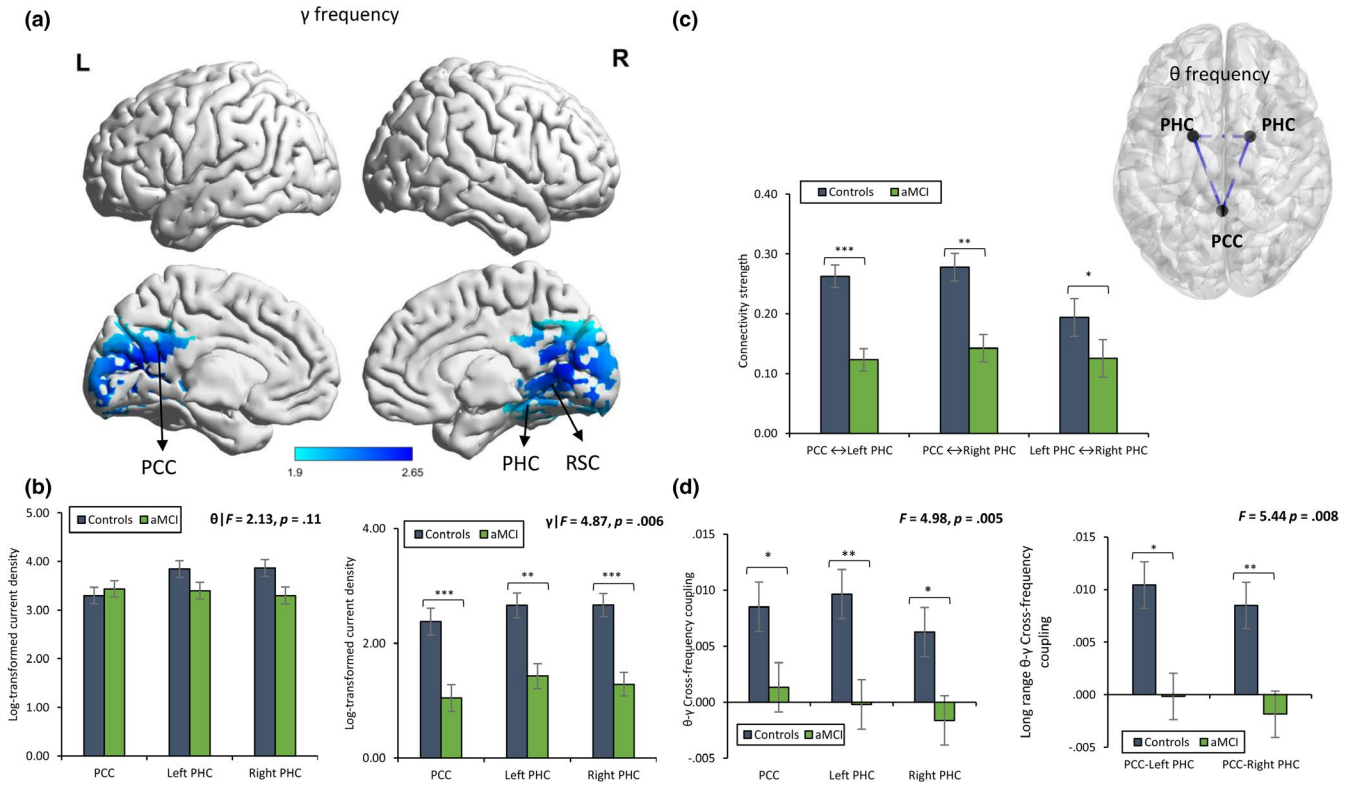

FIGURE 3 (a) Whole-brain analysis shows a significant decrease for the γ frequency band at the posterior cingulate cortex, retrosplenial cortex, and parahippocampus for aMCI patients in comparison to control participants. (b) A comparison for the θ frequency band did not show a significant difference between aMCI patients in comparison to control participants for the posterior cingulate cortex, the left and right parahippocampus. A significant reduction in γ power was obtained for the posterior cingulate cortex, the left and right parahippocampus for aMCI patients in comparison to control participants. (c) Decreased phase coherence between the posterior cingulate cortex, the left parahippocampus, and right parahippocampus for aMCI patients in comparison to control participants. (d) Reduced θ–γ phase–amplitude coupling was obtained for the posterior cingulate cortex, the left parahippocampus, and right parahippocampus for aMCI patients in comparison to control participants. $^*p < 0.05$; $^{**}p < 0.01$; $^{***}p < 0.001$ (e) Reduced θ-γ long-range phase–amplitude coupling was obtained between posterior cingulate cortex and, the left parahippocampus, as well as for the posterior cingulate cortex and right parahippocampus for aMCI patients in comparison to control participants. $^*p < 0.05$; $^{**}p < 0.01$; $^{***}p < 0.001$; posterior cingulate cortex (PCC), retrosplenial cortex (RSC), and parahippocampus (PHC)

A linear discriminant analysis for the γ frequency band including the current density for the PCC, the left and right parahippocampus further showed a strong differentiation between the aMCI and control participants ($\Lambda = 0.71$; $\chi^2(3) = 12.43$, $p = 0.006$). For the discriminant analysis, the PCC ($\Lambda = 0.80$; $F(1,38) = 9.30$, $p = 0.004$), the left parahippocampus ($\Lambda = 0.82$; $F(1,38) = 8.24$, $p = 0.007$), and right parahippocampus ($\Lambda = 0.74$; $F(1,38) = 13.34$, $p = 0.001$) all contribute to the model and were able to correctly classify 85% of aMCI patients as aMCI and 80% of control participants as control or 82.5% over both groups.

3.2.3 | Lagged phase coherence

Comparing patients with aMCI and control participants yielded a significant effect in connectivity for the θ frequency band ($F = 2.11$, $p = 0.015$). That is, decreased lagged phase coherence was obtained between the PCC, and the left and right parahippocampus for the aMCI group (see Figure 3c). No significant effect was obtained when comparing patients with aMCI and control participants for the δ, α, β, and γ frequency band.

3.2.4 | Cross-frequency coupling and long-range phase–amplitude coupling

When comparing patients with aMCI and control participants, an overall significant effect was obtained in θ-γ cross-frequency coupling ($F(3,36) = 4.98$, $p = 0.005$, $\eta^2 = 0.29$; Figure 3d). For PCC ($F(1,38) = 5.32$, $p = 0.027$, $\eta^2 = 0.12$), and the left parahippocampus ($F(1,38) = 11.02$, $p = 0.002$, $\eta^2 = 0.23$) and right parahippocampus ($F(1,38) = 5.81$, $p = 0.021$, $\eta^2 = 0.13$), a significant decrease in nesting was revealed for the aMCI patients (PCC: 0.001 ± 0.008; left HIP: -0.0002 ± 0.008; right HIP: -0.002 ± 0.006) in

comparison to control participants (PCC: 0.009 ± 0.011; left HIP: 0.010 ± 0.010; right HIP: 0.006 ± 0.013).

In addition, long-range phase–amplitude coupling between the amplitude of the γ band of the PCC, and the θ phase of left and right parahippocampus, respectively, showed a significant effect when comparing aMCI patients and control participants ($F(2,37) = 5.44$, $p = 0.008$, $\eta^2 = 0.23$). For both the long-range phase–amplitude coupling between the PCC and left parahippocampus ($F(1,38) = 4.62$, $p = 0.038$, $\eta^2 = 0.11$) and between the PCC and right parahippocampus ($F(1,38) = 7.37$, $p = 0.010$, $\eta^2 = 0.16$), a significant effect was obtained. A significant decrease in long-range phase–amplitude coupling was revealed for the aMCI patients (PCC-left HIP: −0.0001 ± 0.017; PCC-right HIP: −0.002 ± 0.014) in comparison to control participants (PCC-left HIP: 0.010 ± 0.014; PCC-right HIP: 0.009 ± 0.010).

3.2.5 | Correlation between regions of interest and behavioral assessments

A Pearson correlation between the CVLT-II overall score and the current density for γ frequency revealed a significant positive association for the PCC ($r(40) = 0.44$, $p = 0.005$), the left parahippocampus ($r(40) = 0.33$, $p = 0.038$), and the right parahippocampus ($r(40) = 0.38$, $p = 0.017$). After a Bonferroni correction for multiple comparisons (corrected for the three regions of interest), the effect only remained in the PCC. This effect demonstrates that the higher the score on the overall CVLT, the more γ power was present in the PCC (see Figure 4). This effect was mediated by the subscales *Long-delay (free recall)* and *Long-delay (cued recall)*, while no significant correlation was obtained for the subscales *Free recall (list A)*, *Free recall (list B)*, *Short Recall (free recall)*, *Short Recall (cued recall)*, and *Long-delay (recognition)*. For the subscales, we see that the effect was stronger for the PCC than for the left and right parahippocampus. After a Bonferroni correction for multiple comparisons (correct for the 3 regions of interest × the 7 subscales), the effect only remained in the PCC (see Table 1).

A similar analysis between CVLT-II overall score and long-range phase–amplitude coupling between the amplitude of the γ band of the PCC, and the θ phase of left and right parahippocampus, respectively, showed a significant effect for the left parahippocampus ($r(40) = 0.32$, $p = 0.04$). No effect was obtained for the right parahippocampus ($r(40) = 0.28$, $p = 0.08$). After a Bonferroni correction for multiple comparisons (corrected for the two long-range phase–amplitude coupling), the effect for the left parahippocampus did not remain. This effect between the PCC and for the left parahippocampus was mediated by the subscales *Long-delay (free recall)* and *Long-delay (cued recall)*, while no significant correlation was obtained for the subscales *Free recall (list A)*, *Free recall (list B)*, *Short Recall (free recall)*, *Short Recall (cued recall)*, and *Long-delay (recognition)* (see Table 1). After a Bonferroni correction for multiple comparisons (correct for the 3 regions of interest × the 7 subscales), the effect only remained in the *Long-delay (recognition)* and the long-range phase–amplitude coupling between the amplitude of the γ band of the PCC and the θ phase of left parahippocampus.

A Pearson correlation between the current density for γ frequency and the D-KEFS revealed no significant effect for the PCC ($r(40) = -0.13$, $p = 0.44$), the left parahippocampus ($r(40) = -0.14$, $p = 0.39$), and the right parahippocampus ($r(40) = -0.25$, $p = 0.12$). In addition, the subscales of the D-KEFS, namely *Color naming*, *Word reading*, *Inhibition*, and *Inhibition switching* did not show an effect. See Table 2.

A correlation analysis between the D-KEFS and long-range phase–amplitude coupling between the amplitude of the γ band of the PCC, and the θ phase of left parahippocampus

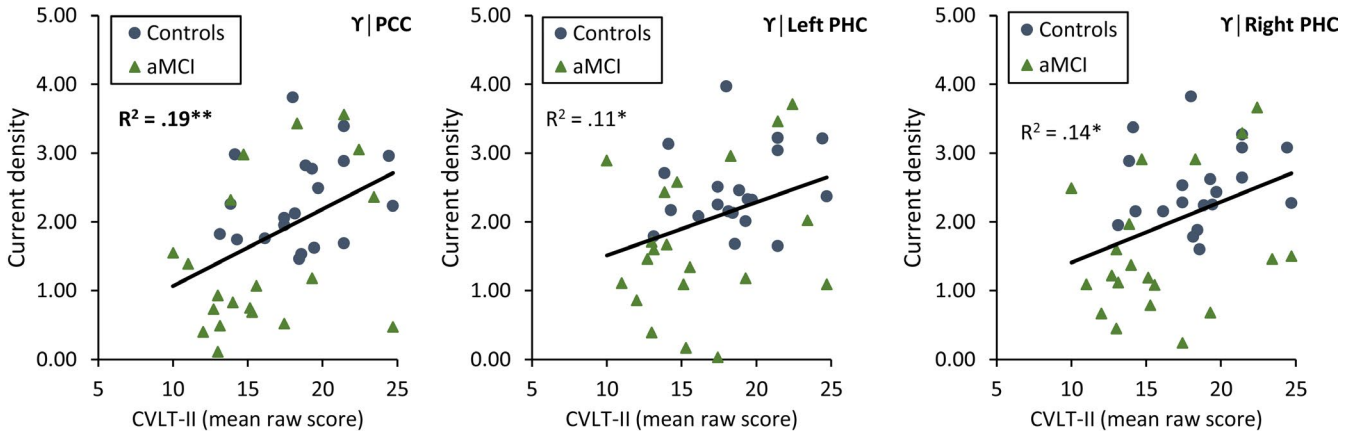

FIGURE 4 A significant positive correlation was demonstrated between CVLT-II and the current density for the posterior cingulate cortex, the left parahippocampus, and right parahippocampus. *$p < 0.05$; **$p < 0.01$; ***$p < 0.001$; posterior cingulate cortex (PCC), parahippocampus (PHC)

TABLE 1 Correlations between CVLT-II subscales and the current density for the posterior cingulate cortex (PCC), the left parahippocampus (PHC), and right parahippocampus (PHC). Correlations between CVLT-II subscales and the long-range phase–amplitude coupling for between the PCC and the left PHC as well as PCC and the right PHC

	PCC	Left PHC	Right PHC
Current density for gamma			
Free recall (list A)	0.31	0.18	0.24
Free recall (list B)	0.22	0.20	0.27
Short-delay (free recall)	0.22	0.25	0.29
Short-delay (cued recall)	0.22	0.11	0.17
Long-delay (free recall)	0.55**	0.42**	0.45**
Long-delay (cued recall)	0.51**	0.39*	0.39*
Long-delay (recognition)	0.17	0.18	0.15
	PCC–Left PHC	**PCC–Right PHC**	
Long-range phase–amplitude coupling			
Free recall (list A)	0.15	0.19	
Free recall (list B)	0.23	0.32	
Short-delay (free recall)	0.29	0.41	
Short-delay (cued recall)	0.21	0.04	
Long-delay (free recall)	0.43**	0.17	
Long-delay (cued recall)	0.52**	0.11	
Long-delay (recognition)	0.17	0.13	

*$p < 0.05$; **$p < 0.01$.

TABLE 2 Correlations between DKEFS subscales and the current density for the posterior cingulate cortex (PCC), the left parahippocampus (PHC), and right parahippocampus (PHC). Correlations between DKEFS subscales and the long-range phase–amplitude coupling for between the PCC and the left PHC as well as PCC and the right PHC

	PCC	Left PHC	Right PHC
Current density: DKEFS for gamma			
Color naming	−0.25	−0.27	−0.29
Word reading	−0.35	−0.31	−0.31
Inhibition	−0.25	−0.27	−0.32
Inhibition switching	−0.21	−0.23	−0.27
Mean raw scores	−0.26	−0.28	−0.31
	PCC–Left PHC	**PCC–Right PHC**	
Long-range phase–amplitude coupling			
Color naming	−08	−0.22	
Word reading	−14	−11	
Inhibition	−23	−0.07	
Inhibition switching	−13	0.09	
Mean raw scores	−0.17	0.03	

($r(40) = -0.17$, $p = 0.31$), and right parahippocampus ($r(40) = 0.03$, $p = 0.85$), respectively, showed no significant effect. In addition, the subscales of the D-KEFS, namely *Color naming*, *Word reading*, *Inhibition*, and *Inhibition switching*, did not show an effect. See Table 2.

3.2.6 | Correlation between lagged phase coherence and behavioral assessments

A correlation for the CVLT-II overall score with the lagged phase coherence between the PCC and the left

parahippocampus, PCC and the right parahippocampus, and the left and right parahippocampus was calculated for the θ bands. This analysis revealed a significant positive correlation between the PCC and the left ($r = 0.42$, $p = 0.032$) and right parahippocampus ($r = 0.39$, $p = 0.044$), respectively, for the θ frequency band. No effect was obtained between the left and right parahippocampus. This effect was mainly driven by the subscales *Long-delay (free recall)* and *Long-delay (cued recall)*, as a similar effect was revealed showing a positive correlation between the PCC and the left (free: $r = 0.45$, $p = 0.023$; cued: $r = 0.39$, $p = 0.044$) and right parahippocampus (free: $r = 0.41$, $p = 0.036$; cued: $r = 0.38$, $p = 0.048$), respectively, for the θ frequency band (see Figure 5). No significant correlation was obtained for the subscales *Free recall (list A)*, *Free recall (list B) Short Recall (free recall)*, *Short Recall (cued recall)*, and *Long-delay (recognition)*.

A similar analysis was conducted for the D-KEFS revealing no significant correlation between the PCC and the left parahippocampus, PCC and the right parahippocampus, and the left and right parahippocampus for the θ bands. Also, the subscales of the D-KEFS, namely *Color naming*, *Word reading*, *Inhibition*, and *Inhibition switching*, did not show an effect (Table 3).

3.2.7 | Correlation between θ-γ phase–amplitude coupling and behavioral assessments

A Pearson correlation between phase–amplitude coupling and the CVLT-II overall score revealed a significant positive association for the PCC ($r(40) = 0.46$, $p = 0.004$), indicating the higher the score on the CVLT-II the stronger the θ-γ phase–amplitude coupling. No significant effect was obtained for

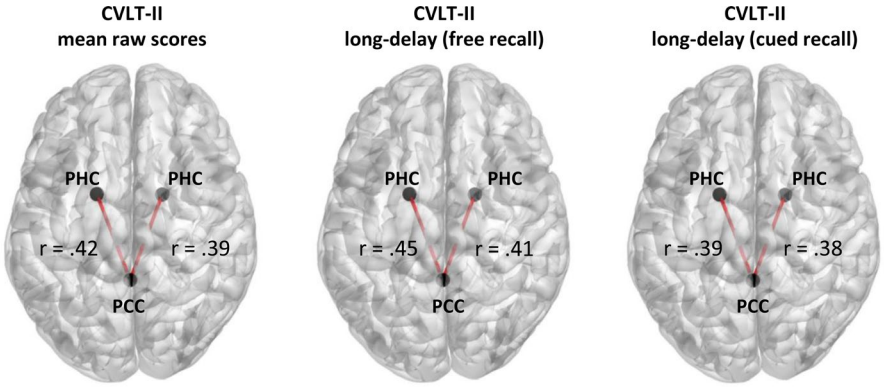

FIGURE 5 A significant positive correlation between phase coherence between the posterior cingulate cortex, and, respectively, the left and right parahippocampus, and the CVLT-II as well as CVLT-II subscales long delay (cued and free recall). *$p < 0.05$; **$p < 0.01$; ***$p < 0.001$; posterior cingulate cortex (PCC) and parahippocampus (PHC)

TABLE 3 Correlations between CVLT-II subscales as well as the DKEFS subscales and the θ-γ phase–amplitude for the posterior cingulate cortex (PCC), the left parahippocampus (PHC), and right parahippocampus (PHC)

	PCC	Left PHC	Right PHC
θ-γ phase–amplitude			
Free recall (list A)	0.36	0.29	0.11
Free recall (list B)	0.03	0.23	0.27
Short-delay (free recall)	0.22	−0.08	0.18
Short-delay (cued recall)	0.14	0.40	0.09
Long-delay (free recall)	0.68***	0.29	0.24
Long-delay (cued recall)	0.63***	0.11	0.22
Long-delay (recognition)	0.29	0.18	0.37
	PCC	**Left PHC**	**Right PHC**
θ-γ phase–amplitude			
Color naming	−0.05	−0.27	−0.20
Word reading	−0.07	−0.28	−0.19
Inhibition	−0.12	−0.05	−0.06
Inhibition switching	−0.01	0.08	0.04
Mean raw scores	−0.04	0.02	−0.01

*$p < 0.05$; **$p < 0.01$; *** $p < 0.0001$.

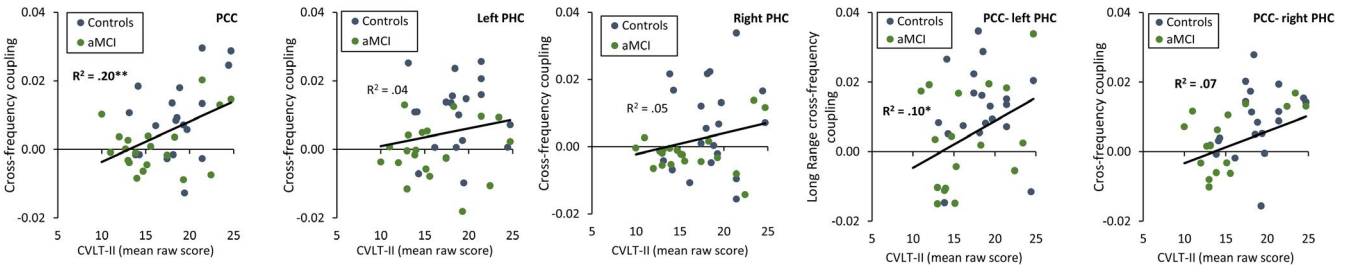

FIGURE 6 A significant positive correlation was revealed between CVLT-II and θ–γ phase–amplitude coupling for the posterior cingulate cortex, the left parahippocampus, and right parahippocampus. *$p < 0.05$; **$p < 0.01$; ***$p < 0.001$; posterior cingulate cortex (PCC), parahippocampus (PHC)

the left parahippocampus ($r(40) = 0.19$, $p = 0.23$) and right parahippocampus ($r(40) = 0.23$, $p = 0.16$) (see Figure 6). After a Bonferroni correction for multiple comparisons (corrected for the 3 regions of interest), the effect remained for the PCC.

A closer look at the data revealed that the effect for the θ-γ phase–amplitude coupling at the PCC was mainly driven by the subscales *Free recall (list A)* ($r(40) = 0.36$, $p = 0.024$), *Long-delay (free recall)* ($r(40) = 0.68$, $p < 0.001$), and *Long-delay (cued recall)* ($r(40) = 0.63$, $p < 0.001$), indicating the higher the scores on these subscales the stronger the θ-γ phase–amplitude coupling. No effect was revealed for the subscales *Free recall (list B)* ($r(40) F = 0.023$ $p = 0.84$), *Short Recall (free recall)* ($r(40) = 0.22$, $p = 0.18$), *Short Recall (cued recall)* ($r(40) = 0.14$, $p = 0.39$), and *Long-delay (recognition)* ($r(40) = 0.29$, $p = 0.07$). After a Bonferroni correction for multiple comparisons (correct for the 3 regions of interest × the 7 subscales), the effect only remained for *Long-delay (free recall)* and *Long-delay (cued recall)*. See Table 3.

No significant effects were obtained for the correlations between the different subscale of the CVLT-II and the left and right parahippocampus.

A similar analysis between the D-KEFS and θ-γ phase–amplitude coupling for PCC ($r(40) = -0.04$, $p = 0.79$), the left parahippocampus ($r(40) = 0.02$, $p = 0.90$), and right parahippocampus ($r(40) = -0.01$, $p = 0.95$), respectively, revealed no significant effect. Also, for the subscales of the D-KEFS, namely *Color* naming, Word *reading*, *Inhibition*, and *Inhibition switching*, no significant effect was obtained with θ-γ phase–amplitude coupling for PCC, the left parahippocampus, and right parahippocampus. See Table 3.

4 | DISCUSSION

We examined the effect of aMCI oscillatory activity in the present study, demonstrating decreased γ power in aMCI patients in comparison to control participants that goes together with reduced θ coherence between the PCC and parahippocampus, which were associated with altered cognitive performance. In addition, changes in cross-frequency coupling between θ and γ oscillations in the PCC and parahippocampus were observed in aMCI patients, which were also associated with altered cognitive performance.

Our data showed a decrease in γ power in the PCC and the left and right parahippocampus for aMCI patients. These specific areas for the γ power can discriminate between aMCI and control participants with 85% accuracy. This is in line with the results of earlier studies, indicating that EEG is a reliable method for the prediction of cognitive decline (Gouw et al., 2017; Klassen et al., 2011; Prichep et al., 2006). Previous memory research indicates that successful retrieval is related to increase in γ-band power in the PCC (Lega et al., 2017). Indeed, γ oscillations have been suggested to cause the (para)hippocampal reinstatement of memory representations in PCC (Nyhus & Curran, 2010). Recent research has further demonstrated that increased γ-frequency ripple oscillations within the human parahippocampus mediate successful memory retrieval (Vaz et al., 2019). Contrarily, a decrease in γ oscillations could suggest the opposite phenomenon, i.e., making it harder for aMCI patients to successfully retrieve information. This idea is consistent with our present findings that decreased γ power in the PCC and the left and right parahippocampus corresponds to a lower score on the CVLT, specifically long delayed recall. Unlike previous EEG studies, our data did not show a slowing of brain electrical activity reflected by θ power increases and α power decreases (van Straaten et al., 2014). This effect was, however, revealed in patients with dementia due to AD. It is possible that this particular outcome only occurs at later stages in the clinical progression from aMCI to AD. This would be consistent with the idea that aMCI is an intermediate stage between healthy controls and dementia patients (Gouw et al., 2017; van der Hiele et al., 2007).

Furthermore, we observed changes in the occipital lobe for patients with aMCI. Although this was not hypothesized, previous research has already indicated that in the early clinical AD stage, one of the symptoms observed in addition to memory decline is progressive impairment in the visual domain that goes together with changes in the occipital lobe

(Cooley et al., 2015; Mendola et al., 1995; Sanabria-Diaz et al., 2013). Interestingly, we do not see changes in the lateral parietal or medial frontal cortex. Previous research on episodic memory has revealed the involvement of these areas in memory consolidation and retrieval (Rugg & King, 2018; Tonegawa et al., 2018). Yet, it is less clear what role(s) the lateral parietal or midline frontal cortex play(s) in patients with aMCI or AD.

Evidence for disrupted structural and functional connectivity in AD patients suggests that memory deficits are related to disconnection syndrome (Sorg et al., 2007). In patients with aMCI, reduced functional connectivity in fMRI has been observed in prodromal stages of AD (Celone et al., 2006), especially during rest (Wang et al., 2006). This is in accordance with our findings of decreased coherence between the PCC and parahippocampus in the θ frequency band in aMCI patients. The θ frequency band is of specific interest as it has previously been associated with successful memory retrieval (Lega et al., 2017). Reduced phase coherence between the PCC and parahippocampus in the θ band could explain why aMCI patients have more difficulty retrieving stored information. Indeed, our data show that decreased coherence within the θ frequency band goes together with a lower score on the CVLT, specifically long delayed recall. No association was obtained between the DKEFS and coherence within the θ band, suggesting that the connection between PCC and parahippocampus reflects difficulties in episodic memory performance (as measured with CVLT) rather than processing speed and interference in general (as measured by the DKEFS).

Our data thus suggest that θ oscillatory coherence between the parahippocampus and PCC is important for memory performance. That is, altered long-term memory is reflected in θ phase coherence between the PCC and parahippocampus in aMCI patients along with decreased θ–γ phase–amplitude coupling. Previous research already indicates that θ phase coupling may provide a scaffold for interregional coordinated activity (Fell & Axmacher, 2011). This fits with the idea that θ oscillations are carrier waves for γ, which bears the actual information, and that this transmission is disrupted in aMCI patients (Lopez-Madrona et al., 2018). However, θ–γ phase–amplitude coupling correlated only with long-delayed recall as measured with CVLT for the PCC, not for the left and right parahippocampus. Interestingly, previous research suggests that (para)hippocampal θ modulates γ activity in PCC and the precuneus while the reverse was not true (Hebscher et al., 2019). Our findings support this idea that the parahippocampus is coordinating neocortical activity via θ phase coherence while γ is of local importance in stimulus-specific information processing (Hebscher et al., 2019). Indeed, we demonstrated changes in γ oscillations in the PCC as well as decreased θ phase coherence that altered long-term memory performance.

A limitation of this study is the low resolution of the source localization and a lack of subject-specific anatomical forward models. This is sufficient for source reconstruction but results in greater uncertainty in source localization and decreased anatomical precision, and thus the spatial precision of the present study is considerably lower than that of functional MRI. Nevertheless, eLORETA has received considerable validation from studies combining LORETA with other, more established localization methods—including fMRI (Mulert et al., 2004; Vitacco et al., 2002), structural MRI (Worrell et al., 2000), and positron emission tomography (PET) (Dierks et al., 2000; Pizzagalli et al., 2004; Zumsteg et al., 2005) – and was used in previous studies to detect activity in, for example, the (para)hippocampus (Vanneste et al., 2010; 2011; Zaehle et al., 2007). Further eLORETA validation has been based on accepting as ground truth the localization findings obtained from invasive, implanted depth electrodes, in which case there are several studies in epilepsy (Zumsteg et al., 2006a; Zumsteg, Lozano, Wieser, et al., 2006) and cognitive ERPs (Volpe et al., 2007). It is worth emphasizing that deep structures such as the anterior cingulate cortex (Pizzagalli et al., 2001) and medial temporal lobes (Zumsteg et al., 2006b) can be correctly localized with these methods. The validity of detecting the involvement of the PCC using 64 electrodes EEG was already illustrated in previous research using combined EEG-fMRI and by intracranial recording, PET, and MRI suggesting the reliability of our findings (Carpenter-Thompson et al., 2014; Langguth et al., 2006; Neuner et al., 2014; Sedley et al., 2015; Vanneste & De Ridder, 2016). However, further research could improve spatial precision and accuracy could be achieved using high-density EEG (e.g., 128 or 256 electrodes) and subject-specific head models, and MEG recordings. Future research needs to replicate these findings in a large population including subject diagnosed with AD to confirm our findings.

Intrinsic brain activity in aMCI is central for understanding the physiology of episodic memory. The PCC and parahippocampus is considered a major cortical hub in the human brain because it maintains dense connectivity to widespread regions involved in multiple memory functions and is one of the cortical regions most vulnerable to AD (Huang et al., 2019; Leech & Sharp, 2014). The present study reinforces this idea. Taken together, our results show that parahippocampus and PCC interact via θ–γ coupling that correlates with memory recollection, but that this is altered in aMCI patients. Hence, this study revealed novel information concerning concomitant oscillations and differences in a network centered on the PCC in aMCI patients versus elderly people with no memory decline, providing a candidate mechanism for this slow but significant memory decline. The results of this study represent the first direct link between memory research on one hand and clinical studies on the other.

DATA SHARING

Data are shared upon request.

CONFLICTS OF INTEREST

The authors have no conflicts of interest to report.

AUTHOR CONTRIBUTIONS

S.V. design, writing, and data analysis; A.L. data collection and data analysis; S.L.M. data collection and data analysis; I.H.R. writing; W.T.T. design and writing.

PEER REVIEW

The peer review history for this article is available at https://publons.com/publon/10.1111/ejn.15189.

ORCID

Sven Vanneste https://orcid.org/0000-0003-1513-5752

REFERENCES

Addante, R. J., Watrous, A. J., Yonelinas, A. P., Ekstrom, A. D., & Ranganath, C. (2011). Prestimulus theta activity predicts correct source memory retrieval. *Proceedings of the National Academy of Sciences of the Unites States of America*, *108*, 10702–10707. https://doi.org/10.1073/pnas.1014528108

Bloomfield, P. (2013). *Fourier analysis of time series: An introduction* (2nd ed.). Wiley-Interscience.

Canolty, R. T., Edwards, E., Dalal, S. S., Soltani, M., Nagarajan, S. S., Kirsch, H. E., Berger, M. S., Barbaro, N. M., & Knight, R. T. (2006). High gamma power is phase-locked to theta oscillations in human neocortex. *Science*, *313*, 1626–1628. https://doi.org/10.1126/science.1128115

Carpenter-Thompson, J. R., Akrofi, K., Schmidt, S. A., Dolcos, F., & Husain, F. T. (2014). Alterations of the emotional processing system may underlie preserved rapid reaction time in tinnitus. *Brain Research*, *1567*, 28–41. https://doi.org/10.1016/j.brainres.2014.04.024

Celone, K. A., Calhoun, V. D., Dickerson, B. C., Atri, A., Chua, E. F., Miller, S. L., DePeau, K., Rentz, D. M., Selkoe, D. J., Blacker, D., Albert, M. S., & Sperling, R. A. (2006). Alterations in memory networks in mild cognitive impairment and Alzheimer's disease: An independent component analysis. *Journal of Neuroscience*, *26*, 10222–10231. https://doi.org/10.1523/JNEUROSCI.2250-06.2006

Cohen, M. X. (2017). Where does EEG come from and what does it mean? *Trends in Neurosciences*, *40*, 208–218. https://doi.org/10.1016/j.tins.2017.02.004

Colgin, L. L. (2015). Theta-gamma coupling in the entorhinal-hippocampal system. *Current Opinion in Neurobiology*, *31*, 45–50. https://doi.org/10.1016/j.conb.2014.08.001

Congedo, M. (2002) EureKa! (Version 3.0) [Computer Software]. NovaTech EEG Inc. Freeware available at www.NovaTechEEG

Congedo, M., John, R. E., De Ridder, D., Prichep, L., & Isenhart, R. (2010). On the "dependence" of "independent" group EEG sources; an EEG study on two large databases. *Brain Topography*, *23*, 134–138. https://doi.org/10.1007/s10548-009-0113-6

Cooley, S. A., Cabeen, R. P., Laidlaw, D. H., Conturo, T. E., Lane, E. M., Heaps, J. M., Bolzenius, J. D., Baker, L. M., Salminen, L. E., Scott, S. E., & Paul, R. H. (2015). Posterior brain white matter abnormalities in older adults with probable mild cognitive impairment. *Journal of Clinical and Experimental Neuropsychology*, *37*, 61–69. https://doi.org/10.1080/13803395.2014.985636

Delis, D. C., Kaplan, E., & Kramer, J. H. (2001). *Delis-Kaplan executive function system (D-KEFS)*. Psychological Corporation.

Dierks, T., Jelic, V., Pascual-Marqui, R. D., Wahlund, L., Julin, P., Linden, D. E., Maurer, K., Winblad, B., & Nordberg, A. (2000). Spatial pattern of cerebral glucose metabolism (PET) correlates with localization of intracerebral EEG-generators in Alzheimer's disease. *Clinical Neurophysiology*, *111*, 1817–1824. https://doi.org/10.1016/S1388-2457(00)00427-2

Drzezga, A., Becker, J. A., Van Dijk, K. R., Sreenivasan, A., Talukdar, T., Sullivan, C., Schultz, A. P., Sepulcre, J., Putcha, D., Greve, D., Johnson, K. A., & Sperling, R. A. (2011). Neuronal dysfunction and disconnection of cortical hubs in non-demented subjects with elevated amyloid burden. *Brain*, *134*, 1635–1646. https://doi.org/10.1093/brain/awr066

Elman, J. A., Madison, C. M., Baker, S. L., Vogel, J. W., Marks, S. M., Crowley, S., O'Neil, J. P., & Jagust, W. J. (2016). Effects of beta-amyloid on resting state functional connectivity within and between networks reflect known patterns of regional vulnerability. *Cerebral Cortex*, *26*, 695–707.

Fell, J., & Axmacher, N. (2011). The role of phase synchronization in memory processes. *Nature Reviews Neuroscience*, *12*, 105–118. https://doi.org/10.1038/nrn2979

Finn, E. S., Shen, X., Scheinost, D., Rosenberg, M. D., Huang, J., Chun, M. M., Papademetris, X., & Constable, R. T. (2015). Functional connectome fingerprinting: Identifying individuals using patterns of brain connectivity. *Nature Neuroscience*, *18*, 1664–1671. https://doi.org/10.1038/nn.4135

Fuchs, M., Kastner, J., Wagner, M., Hawes, S., & Ebersole, J. S. (2002). A standardized boundary element method volume conductor model. *Clinical Neurophysiology*, *113*, 702–712. https://doi.org/10.1016/S1388-2457(02)00030-5

Gabrieli, J. D. E., Ghosh, S. S., & Whitfield-Gabrieli, S. (2015). Prediction as a humanitarian and pragmatic contribution from human cognitive neuroscience. *Neuron*, *85*, 11–26. https://doi.org/10.1016/j.neuron.2014.10.047

Gouw, A. A., Alsema, A. M., Tijms, B. M., Borta, A., Scheltens, P., Stam, C. J., & van der Flier, W. M. (2017). EEG spectral analysis as a putative early prognostic biomarker in nondemented, amyloid positive subjects. *Neurobiology of Aging*, *57*, 133–142. https://doi.org/10.1016/j.neurobiolaging.2017.05.017

Hebscher, M., Meltzer, J. A., & Gilboa, A. (2019). A causal role for the precuneus in network-wide theta and gamma oscillatory activity during complex memory retrieval. *Elife*, *8*. https://doi.org/10.7554/eLife.43114

Hedden, T., Van Dijk, K. R., Becker, J. A., Mehta, A., Sperling, R. A., Johnson, K. A., & Buckner, R. L. (2009). Disruption of functional connectivity in clinically normal older adults harboring amyloid burden. *The Journal of Neuroscience*, *29*, 12686–12694. https://doi.org/10.1523/JNEUROSCI.3189-09.2009

Holm, S. (1979). A simple sequential rejective multiple test procedure. *Scandinavian Journal of Statistics*, *6*, 65–70.

Huang, Y., Hullfish, J., De Ridder, D., & Vanneste, S. (2019). Meta-analysis of functional subdivisions within human posteromedial cortex. *Brain Structure & Function*, *224*, 435–452. https://doi.org/10.1007/s00429-018-1781-3

Jatoi, M. A., Kamel, N., Malik, A. S., & Faye, I. (2014). EEG based brain source localization comparison of sLORETA and eLORETA.

Australasian Physical and Engineering Sciences in Medicine, *37*, 713–721. https://doi.org/10.1007/s13246-014-0308-3

Jurcak, V., Tsuzuki, D., & Dan, I. (2007). 10/20, 10/10, and 10/5 systems revisited: Their validity as relative head-surface-based positioning systems. *NeuroImage*, *34*, 1600–1611. https://doi.org/10.1016/j.neuroimage.2006.09.024

Kennedy, K. M., Rodrigue, K. M., Devous, M. D. Sr, Hebrank, A. C., Bischof, G. N., & Park, D. C. (2012). Effects of beta-amyloid accumulation on neural function during encoding across the adult lifespan. *NeuroImage*, *62*, 1–8. https://doi.org/10.1016/j.neuroimage.2012.03.077

Klassen, B. T., Hentz, J. G., Shill, H. A., Driver-Dunckley, E., Evidente, V. G., Sabbagh, M. N., Adler, C. H., & Caviness, J. N. (2011). Quantitative EEG as a predictive biomarker for Parkinson disease dementia. *Neurology*, *77*, 118–124. https://doi.org/10.1212/WNL.0b013e318224af8d

Lancaster, J. L., Woldorff, M. G., Parsons, L. M., Liotti, M., Freitas, C. S., Rainey, L., Kochunov, P. V., Nickerson, D., Mikiten, S. A., & Fox, P. T. (2000). Automated Talairach atlas labels for functional brain mapping. *Human Brain Mapping*, *10*, 120–131. https://doi.org/10.1002/1097-0193(200007)10:3<120:AID-HBM30>3.0.CO;2-8

Langa, K. M., & Levine, D. A. (2014). The diagnosis and management of mild cognitive impairment: A clinical review. *JAMA*, *312*, 2551–2561. https://doi.org/10.1001/jama.2014.13806

Langguth, B., Eichhammer, P., Kreutzer, A., Maenner, P., Marienhagen, J., Kleinjung, T., Sand, P., & Hajak, G. (2006). The impact of auditory cortex activity on characterizing and treating patients with chronic tinnitus–first results from a PET study. *Acta Oto-Laryngologica*, *126*(sup556), 84–88. https://doi.org/10.1080/03655230600895317

Leech, R., & Sharp, D. J. (2014). The role of the posterior cingulate cortex in cognition and disease. *Brain*, *137*, 12–32. https://doi.org/10.1093/brain/awt162

Lega, B., Germi, J., & Rugg, M. (2017). Modulation of oscillatory power and connectivity in the human posterior cingulate cortex supports the encoding and retrieval of episodic memories. *Journal of Cognitive Neuroscience*, *29*, 1415–1432. https://doi.org/10.1162/jocn_a_01133

Lin, Q., Rosenberg, M. D., Yoo, K., Hsu, T. W., O'Connell, T. P., & Chun, M. M. (2018). Resting-state functional connectivity predicts cognitive impairment related to Alzheimer's disease. *Frontiers in Aging Neuroscience*, *10*, 94. https://doi.org/10.3389/fnagi.2018.00094

Logan, J. M., Sanders, A. L., Snyder, A. Z., Morris, J. C., & Buckner, R. L. (2002). Under-recruitment and nonselective recruitment: Dissociable neural mechanisms associated with aging. *Neuron*, *33*, 827–840. https://doi.org/10.1016/S0896-6273(02)00612-8

Lopez-Madrona, V. J., Álvarez-Salvado, E., Moratal, D., Herreras, O., Pereda, E., Mirasso, C. R., & Canals, S. (2018). Gamma oscillations coordinate different theta rhythms in the hippocampus. *bioRxiv*, 418434.

McLachlan, G. J. (2004). *Discriminant analysis and statistical pattern recognition*. Wiley Interscience.

Mendola, J. D., Cronin-Golomb, A., Corkin, S., & Growdon, J. H. (1995). Prevalence of visual deficits in Alzheimer's disease. *Optometry and Vision Science*, *72*, 155–167. https://doi.org/10.1097/00006324-199503000-00003

Moazami-Goudarzi, M., Michels, L., Weisz, N., & Jeanmonod, D. (2010). Temporo-insular enhancement of EEG low and high frequencies in patients with chronic tinnitus. QEEG study of chronic tinnitus patients. *BMC Neuroscience*, *11*, 40. https://doi.org/10.1186/1471-2202-11-40

Mormann, F., Fell, J., Axmacher, N., Weber, B., Lehnertz, K., Elger, C. E., & Fernandez, G. (2005). Phase/amplitude reset and theta-gamma interaction in the human medial temporal lobe during a continuous word recognition memory task. *Hippocampus*, *15*, 890–900. https://doi.org/10.1002/hipo.20117

Mormino, E. C., Brandel, M. G., Madison, C. M., Marks, S., Baker, S. L., & Jagust, W. J. (2012). Abeta Deposition in aging is associated with increases in brain activation during successful memory encoding. *Cerebral Cortex*, *22*, 1813–1823.

Mulert, C., Jager, L., Schmitt, R., Bussfeld, P., Pogarell, O., Moller, H. J., Juckel, G., & Hegerl, U. (2004). Integration of fMRI and simultaneous EEG: Towards a comprehensive understanding of localization and time-course of brain activity in target detection. *NeuroImage*, *22*, 83–94. https://doi.org/10.1016/j.neuroimage.2003.10.051

Neuner, I., Arrubla, J., Werner, C. J., Hitz, K., Boers, F., Kawohl, W., & Shah, N. J. (2014). The default mode network and EEG regional spectral power: A simultaneous fMRI-EEG study. *PLoS One*, *9*, e88214. https://doi.org/10.1371/journal.pone.0088214

Nichols, T. E., & Holmes, A. P. (2002). Nonparametric permutation tests for functional neuroimaging: A primer with examples. *Human Brain Mapping*, *15*, 1–25. https://doi.org/10.1002/hbm.1058

Nyhus, E., & Curran, T. (2010). Functional role of gamma and theta oscillations in episodic memory. *Neuroscience and Biobehavioral Reviews*, *34*, 1023–1035. https://doi.org/10.1016/j.neubiorev.2009.12.014

Oh, H., & Jagust, W. J. (2013). Frontotemporal network connectivity during memory encoding is increased with aging and disrupted by beta-amyloid. *The Journal of Neuroscience*, *33*, 18425–18437. https://doi.org/10.1523/JNEUROSCI.2775-13.2013

Pascual-Marqui, R. D. (2002) Standardized low-resolution brain electromagnetic tomography (sLORETA): Technical details. *Methods and Findings in Experimental and Clinical Pharmacology*, *24*(Suppl D), 5-12.

Pascual-Marqui, R. (2007). Instantaneous and lagged measurements of linear and nonlinear dependence between groups of multivariate time series: Frequency decomposition. http://arxiv.org/abs/0711.1455

Pascual-Marqui, R. D., Lehmann, D., Koukkou, M., Kochi, K., Anderer, P., Saletu, B., Tanaka, H., Hirata, K., John, E. R., Prichep, L., Biscay-Lirio, R., & Kinoshita, T. (2011). Assessing interactions in the brain with exact low-resolution electromagnetic tomography. *Philosophical Transactions of the Royal Society A: Mathematical, Physical and Engineering Sciences*, *369*, 3768–3784. https://doi.org/10.1098/rsta.2011.0081

Petersen, R. C., & Negash, S. (2008). Mild cognitive impairment: An overview. *CNS Spectrums*, *13*, 45–53.

Pizzagalli, D. A., Oakes, T. R., Fox, A. S., Chung, M. K., Larson, C. L., Abercrombie, H. C., Schaefer, S. M., Benca, R. M., & Davidson, R. J. (2004). Functional but not structural subgenual prefrontal cortex abnormalities in melancholia. *Molecular Psychiatry*, *9*(325), 393–405. https://doi.org/10.1038/sj.mp.4001469

Pizzagalli, D., Pascual-Marqui, R. D., Nitschke, J. B., Oakes, T. R., Larson, C. L., Abercrombie, H. C., Schaefer, S. M., Koger, J. V., Benca, R. M., & Davidson, R. J. (2001). Anterior cingulate activity as a predictor of degree of treatment response in major depression: Evidence from brain electrical tomography analysis. *American Journal of Psychiatry*, *158*, 405–415. https://doi.org/10.1176/appi.ajp.158.3.405

Prichep, L. S., John, E. R., Ferris, S. H., Rausch, L., Fang, Z., Cancro, R., Torossian, C., & Reisberg, B. (2006). Prediction of longitudinal

cognitive decline in normal elderly with subjective complaints using electrophysiological imaging. *Neurobiology of Aging*, *27*, 471–481. https://doi.org/10.1016/j.neurobiolaging.2005.07.021

Rosenberg, M. D., Finn, E. S., Scheinost, D., Papademetris, X., Shen, X., Constable, R. T., & Chun, M. M. (2016). A neuromarker of sustained attention from whole-brain functional connectivity. *Nature Neuroscience*, *19*, 165–171. https://doi.org/10.1038/nn.4179

Rugg, M. D., & King, D. R. (2018). Ventral lateral parietal cortex and episodic memory retrieval. *Cortex*, *107*, 238–250. https://doi.org/10.1016/j.cortex.2017.07.012

Sanabria-Diaz, G., Martinez-Montes, E., & Melie-Garcia, L.; Alzheimer's Disease Neuroimaging Initiative. (2013). Glucose metabolism during resting state reveals abnormal brain networks organization in the Alzheimer's disease and mild cognitive impairment. *PLoS One*, *8*, e68860. https://doi.org/10.1371/journal.pone.0068860

Sedley, W., Gander, P. E., Kumar, S., Oya, H., Kovach, C. K., Nourski, K. V., Kawasaki, H., Howard, M. A. 3rd, & Griffiths, T. D. (2015). Intracranial mapping of a cortical tinnitus system using residual inhibition. *Current Biology*, *25*, 1208–1214. https://doi.org/10.1016/j.cub.2015.02.075

Shen, X., Finn, E. S., Scheinost, D., Rosenberg, M. D., Chun, M. M., Papademetris, X., & Constable, R. T. (2017). Using connectome-based predictive modeling to predict individual behavior from brain connectivity. *Nature Protocols*, *12*, 506–518. https://doi.org/10.1038/nprot.2016.178

Siepmann, M., & Kirch, W. (2002). Effects of caffeine on topographic quantitative EEG. *Neuropsychobiology*, *45*, 161–166. https://doi.org/10.1159/000054958

Sorg, C., Riedl, V., Muhlau, M., Calhoun, V. D., Eichele, T., Laer, L., Drzezga, A., Forstl, H., Kurz, A., Zimmer, C., & Wohlschlager, A. M. (2007). Selective changes of resting-state networks in individuals at risk for Alzheimer's disease. *Proceedings of the National Academy of Sciences of the Unites States of America*, *104*, 18760–18765. https://doi.org/10.1073/pnas.0708803104

Spaniol, J., Davidson, P. S., Kim, A. S., Han, H., Moscovitch, M., & Grady, C. L. (2009). Event-related fMRI studies of episodic encoding and retrieval: Meta-analyses using activation likelihood estimation. *Neuropsychologia*, *47*, 1765–1779. https://doi.org/10.1016/j.neuropsychologia.2009.02.028

Sperling, R. A., Aisen, P. S., Beckett, L. A., Bennett, D. A., Craft, S., Fagan, A. M., Iwatsubo, T., Jack, C. R. Jr, Kaye, J., Montine, T. J., Park, D. C., Reiman, E. M., Rowe, C. C., Siemers, E., Stern, Y., Yaffe, K., Carrillo, M. C., Thies, B., Morrison-Bogorad, M., … Phelps, C. H. (2011). Toward defining the preclinical stages of Alzheimer's disease: Recommendations from the National Institute on Aging-Alzheimer's Association workgroups on diagnostic guidelines for Alzheimer's disease. *Alzheimer's & Dementia*, *7*, 280–292. https://doi.org/10.1016/j.jalz.2011.03.003

Sperling, R. A., Karlawish, J., & Johnson, K. A. (2013). Preclinical Alzheimer disease-the challenges ahead. *Nature Reviews Neurology*, *9*, 54–58. https://doi.org/10.1038/nrneurol.2012.241

Summers, M. J., & Saunders, N. L. (2012). Neuropsychological measures predict decline to Alzheimer's dementia from mild cognitive impairment. *Neuropsychology*, *26*, 498–508. https://doi.org/10.1037/a0028576

Tonegawa, S., Morrissey, M. D., & Kitamura, T. (2018). The role of engram cells in the systems consolidation of memory. *Nature Reviews Neuroscience*, *19*, 485–498.

van der Hiele, K., Vein, A. A., Reijntjes, R. H., Westendorp, R. G., Bollen, E. L., van Buchem, M. A., van Dijk, J. G., & Middelkoop, H. A. (2007). EEG correlates in the spectrum of cognitive decline. *Clinical Neurophysiology*, *118*, 1931–1939. https://doi.org/10.1016/j.clinph.2007.05.070

van Straaten, E. C., Scheltens, P., Gouw, A. A., & Stam, C. J. (2014). Eyes-closed task-free electroencephalography in clinical trials for Alzheimer's disease: An emerging method based upon brain dynamics. *Alzheimer's Research & Therapy*, *6*, 86. https://doi.org/10.1186/s13195-014-0086-x

Vanneste, S., & De Ridder, D. (2016). Deafferentation-based pathophysiological differences in phantom sound: Tinnitus with and without hearing loss. *NeuroImage*, *129*, 80–94. https://doi.org/10.1016/j.neuroimage.2015.12.002

Vanneste, S., Plazier, M., van der Loo, E., Van de Heyning, P., & De Ridder, D. (2010). The difference between uni- and bilateral auditory phantom percept. *Clinical Neurophysiology*, *122*(3), 578–587. https://doi.org/10.1016/j.clinph.2010.07.022

Vaz, A. P., Inati, S. K., Brunel, N., & Zaghloul, K. A. (2019). Coupled ripple oscillations between the medial temporal lobe and neocortex retrieve human memory. *Science*, *363*, 975–978. https://doi.org/10.1126/science.aau8956

Vitacco, D., Brandeis, D., Pascual-Marqui, R., & Martin, E. (2002). Correspondence of event-related potential tomography and functional magnetic resonance imaging during language processing. *Human Brain Mapping*, *17*, 4–12. https://doi.org/10.1002/hbm.10038

Volkow, N. D., Logan, J., Fowler, J. S., Wang, G. J., Gur, R. C., Wong, C., Felder, C., Gatley, S. J., Ding, Y. S., Hitzemann, R., & Pappas, N. (2000). Association between age-related decline in brain dopamine activity and impairment in frontal and cingulate metabolism. *The American Journal of Psychiatry*, *157*, 75–80. https://doi.org/10.1176/ajp.157.1.75

Volpe, U., Mucci, A., Bucci, P., Merlotti, E., Galderisi, S., & Maj, M. (2007). The cortical generators of P3a and P3b: A LORETA study. *Brain Research Bulletin*, *73*, 220–230. https://doi.org/10.1016/j.brainresbull.2007.03.003

Voytek, B., & Gazzaley, A. (2013). Stimulating the aging brain. *Annals of Neurology*, *73*, 1–3. https://doi.org/10.1002/ana.23790

Wang, L., Zang, Y., He, Y., Liang, M., Zhang, X., Tian, L., Wu, T., Jiang, T., & Li, K. (2006). Changes in hippocampal connectivity in the early stages of Alzheimer's disease: Evidence from resting state fMRI. *NeuroImage*, *31*, 496–504. https://doi.org/10.1016/j.neuroimage.2005.12.033

Woo, C. W., Chang, L. J., Lindquist, M. A., & Wager, T. D. (2017). Building better biomarkers: Brain models in translational neuroimaging. *Nature Neuroscience*, *20*, 365–377. https://doi.org/10.1038/nn.4478

Worrell, G. A., Lagerlund, T. D., Sharbrough, F. W., Brinkmann, B. H., Busacker, N. E., Cicora, K. M., & O'Brien, T. J. (2000). Localization of the epileptic focus by low-resolution electromagnetic tomography in patients with a lesion demonstrated by MRI. *Brain Topography*, *12*, 273–282.

Zaehle, T., Jancke, L., & Meyer, M. (2007). Electrical brain imaging evidences left auditory cortex involvement in speech and non-speech discrimination based on temporal features. *Behavioral and Brain Functions*, *3*, 63. https://doi.org/10.1186/1744-9081-3-63

Zumsteg, D., Lozano, A. M., & Wennberg, R. A. (2006a). Depth electrode recorded cerebral responses with deep brain stimulation of the anterior thalamus for epilepsy. *Clinical Neurophysiology*, *117*, 1602–1609. https://doi.org/10.1016/j.clinph.2006.04.008

Zumsteg, D., Lozano, A. M., & Wennberg, R. A. (2006b). Mesial temporal inhibition in a patient with deep brain stimulation of the

anterior thalamus for epilepsy. *Epilepsia*, *47*, 1958–1962. https://doi.org/10.1111/j.1528-1167.2006.00824.x

Zumsteg, D., Lozano, A. M., Wieser, H. G., & Wennberg, R. A. (2006). Cortical activation with deep brain stimulation of the anterior thalamus for epilepsy. *Clinical Neurophysiology*, *117*, 192–207. https://doi.org/10.1016/j.clinph.2005.09.015

Zumsteg, D., Wennberg, R. A., Treyer, V., Buck, A., & Wieser, H. G. (2005). H2(15)O or 13NH3 PET and electromagnetic tomography (LORETA) during partial status epilepticus. *Neurology*, *65*, 1657–1660. https://doi.org/10.1212/01.wnl.0000184516.32369.1a

How to cite this article: Vanneste S, Luckey A, McLeod SL, Robertson IH, To WT. Impaired posterior cingulate cortex–parahippocampus connectivity is associated with episodic memory retrieval problems in amnestic mild cognitive impairment. *Eur J Neurosci*. 2021;53:3125–3141. https://doi.org/10.1111/ejn.15189